Direction-of-Arrival Ambiguities Mitigation in Multibeam Leaky-Wave Antennas

Julien Sarrazin, Guido Valerio

Direction-of-Arrival Ambiguities Mitigation in Multibeam Leaky-Wave Antennas

Julien Sarrazin*, Guido Valerio*,
*Sorbonne Université, CNRS, Laboratoire de Génie Electrique et Electronique de Paris, 75252, Paris, France
Université Paris-Saclay, CentraleSupélec, CNRS, Laboratoire de Génie Electrique et Electronique de Paris,
91192, Gif-sur-Yvette, France, julien.sarrazin@sorbonne-universite.fr

***Abstract*—The inherent frequency beam scanning behavior of leaky-wave antennas (LWA) enables estimating directions of arrival (DoA) with a reduced complexity with respect to antenna-array-based DoA estimation. It has been shown recently that making use of multiple fast Floquet harmonics in periodic LWA can drastically reduce the frequency bandwidth required to scan a large angular field of view. However, with this multibeam operation, the columns of the LWA response matrix are not linearly independent which gives rise to ambiguities, i.e., spurious peaks in the MUSIC pseudo spectrum, in the DoA estimation. Indeed, if the number of snapshots and/or SNR is not sufficiently high, DoA ambiguities arise which leads to false detection. To tackle this issue, this paper investigates an approach to make use of signals received by both ports of a 1-D LWA in order to effectively mitigate those ambiguities.**

***Index Terms*—Multibeam leaky-wave antennas, periodic structure, angle-of-arrival estimation, MUSIC.**

I. Introduction

Direction of arrival (DoA) estimation plays a crucial role in positioning system [1] and can also benefit to directional wireless communications which requires DoA knowledge for beam alignment. DoA estimation is classically performed using antenna array with dedicated signal processing [2]. To do so, the signal received by each antenna needs to be processed. This requires therefore a dedicated frond-end and analog-to-digital converter (ADC) per antenna, which increases cost, complexity, and power consumption of the system as the number of antennas in the array gets larger. However, a large antenna array might be necessary to increase the accuracy on the estimated DoAs and/or to increase the number of sources that are resolvable by the system, depending on the estimation algorithm.

Analog phased arrays, thanks to their electronic beam scanning capabilities, can reduce power consumption, since a single ADC is required. This comes however at the expense of a higher hardware complexity because of the required beamforming network which includes active components, such as phase shifters, as numerous as the antennas in the array. This higher complexity can be an issue when considering a large number of antennas, as required at millimeter-wave (mmWave) frequencies.

Leaky-wave antennas (LWA) are an alternative approach to reduce cost, complexity, and power consumption, in DoA estimation systems. LWA makes use of a fast traveling wave inside a partially open waveguide which leaks out of the structure and creates a directional beam without the need for beamforming network. With a single port excitation, a high gain can be achieved by simply increasing the LWA length and controlling the leakage constant [3]. In other words, the complexity of the structure does not scale with increasing DoA resolution capabilities. Furthermore, LWA beams naturally steer with frequency, which enables estimating DoA without any additional active components.

One limitation of LWA in DoA estimation is the necessity to operate over a wide frequency bandwidth to steer the beam across a large field of view (FoV). Several LWA designs at mmWave have been proposed to increase this frequency scanning velocity. In [4], the LWA is loaded with a dense metasurface while in [5], an extra dispersive lens is added to the LWA. The scanning velocity obtained remains however too low for the FoV to be covered with a typical telecommunications frequency channel. At lower frequencies, [6] makes use of both LWA ports in order to achieve a FoV of $40°$ exploiting only the 2.4 GHz WiFi channels while [7] achieves a FoV of about $130°$ using LoRa channels. At mmWave, [8] proposes to use periodic LWAs that support multiple fast spatial harmonics, which generate, for a given frequency, multiple beams in different directions. In doing so, the FoV is divided by the number of beams, i.e., the number of fast spatial harmonics. Thus, each beam needs to span a reduced angular range, hence requiring a reduced frequency bandwidth to do so. [9] and [10] introduce frequency-scanning multibeam LWA designs to assess this scheme. It was observed that leveraging multibeam LWA in DoA estimation is prone to DoA ambiguities.

The goal of this paper is to investigates the effect of jointly using signals received by both ports of a 1-D LWA in order to effectively reduce those ambiguities. Section II briefly introduces the LWA model used in this paper while Section III described the system model used for DoA estimation. Section IV presents the DoA ambiguities mitigation techniques that are assessed in Section V. Conclusions are drawn in Section VI .

II. Leaky-Wave Antenna Model

The multibeam LWA model used in this paper is the antenna introduced in [9], which for convenience is also illustrated in Fig. 1. It consists in a dielectric-filled rectangular waveguide of width 3.5 mm and height 0.762 mm, which is periodically

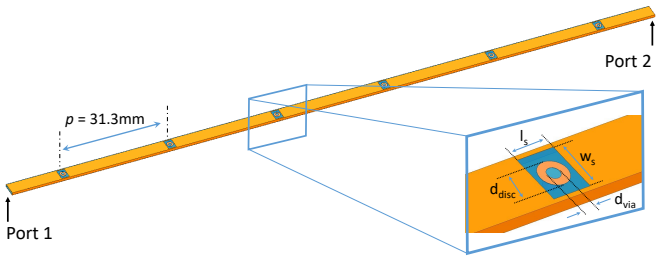

Fig. 1: 6-cells LWA geometry with overall length of 18.78 cm, waveguide width of 3.5 mm, and height of 0.762 mm. Dimensions of rectangular slots with via hole are: $l_s = 3$ mm, $w_s = 2.3$ mm, $d_{via} = 0.8$ mm, and $d_{disc} = 1.7$ mm. The waveguide is filled with dielectric ($\epsilon_r = 2.94$ and $\tan\delta = 0.0012$).

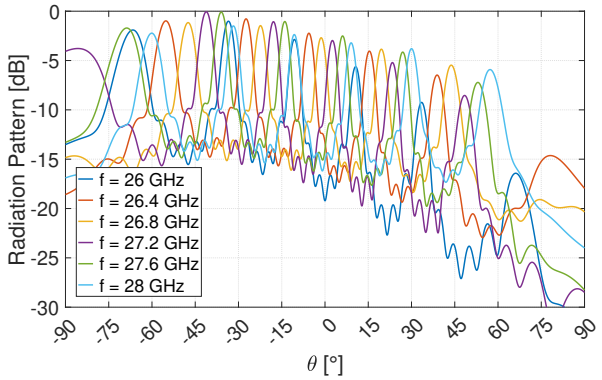

Fig. 2: Normalized radiation pattern of the LWA fed by port 1.

etched by slots inside which there is a via-hole topped with a disc. This unit cell was designed to suppress bandgaps in the structure. Dimensions of the structure and dielectric properties are given in Fig. 1 caption. This LWA contains 6 unit-cells with a period $p = 31.3$ mm, which is large enough to generate between 5 and 6 fast Floquet harmonics that contribute to the far-field radiation in the 26-28 GHz range. The radiation pattern simulated with Ansys HFSS from port 1 excitation is shown in Fig. 2 for a few selected frequencies. The radiation pattern from port 2, not shown here, is the same one with a mirror symmetry with respect to $\theta = 0°$. The -3 dB beamwidth varies between $3.2°$ and $4.5°$ in the $\theta = \pm 45°$ range, and gets progressively larger as beams steer towards end-fire. Up to 6 beams per frequency are visible. Furthermore, as the frequency varies, the multiple beams scan the entire FoV, with the gain dropping as the beams steer towards end-fire, especially towards the $\theta = +90°$ direction. As first shown in [8], operating with multiple beams enables reducing the angular range over which each single beam needs to scan, which in turn greatly reduces the frequency bandwidth required to scan the whole FoV. However, this introduces ambiguities in the DoA estimate among the multiple beams, which can be mitigated to some extent with algorithm such as MUSIC, as seen in next sections.

III. MUSIC System Model

The DoA of D sources impinging on the LWA is estimated using MUSIC algorithm. The system model assumes that the D sources are modulated using a multicarrier scheme, where all subcarriers considered for the DoA estimation convey the same data. Consequently, the signal received by either of the LWA ports can be expressed in frequency domain as:

$$\underbrace{\begin{bmatrix} x_1^{(i)}[k] \\ \vdots \\ x_M^{(i)}[k] \end{bmatrix}}_{\mathbf{x}^{(i)}} = \underbrace{\begin{bmatrix} a_1^{(i)}(\theta_1) & \dots & a_1^{(i)}(\theta_D) \\ \vdots & \ddots & \vdots \\ a_M^{(i)}(\theta_1) & \dots & a_M^{(i)}(\theta_D) \end{bmatrix}}_{\mathbf{A}^{(i)}} \cdot \underbrace{\begin{bmatrix} s_1[k] \\ \vdots \\ s_D[k] \end{bmatrix}}_{\mathbf{s}} + \underbrace{\begin{bmatrix} z_1^{(i)}[k] \\ \vdots \\ z_M^{(i)}[k] \end{bmatrix}}_{\mathbf{z}^{(i)}} \tag{1}$$

where $i = 1, 2$ is the LWA port number. $\mathbf{x}^{(i)} \in \mathbb{C}^{M\times 1}$ is the data vector received by port i where M is the number of frequency samples and $k = 1, \dots, K$ is the kth snapshot among K. $\mathbf{A}^{(i)} \in \mathbb{C}^{M\times D}$ is the LWA response matrix of port i where each column represents the LWA frequency response to an incident plane wave of AoA $\theta_{d=1,\dots,D}$. $\mathbf{s} \in \mathbb{C}^{D\times 1}$ is the source vector, i.e., the complex amplitude of the D sources. $\mathbf{z} \in \mathbb{C}^{M\times 1}$ is a complex Additive White Gaussian Noise (AWGN) vector with uncorrelated components.

It is to be noted that M represents the number of frequency samples, e.g., the number of subcarriers used in the D sources, as opposed to the number of antennas in a typical linear-array-based MUSIC scenario.

To estimate the DoA of the D sources, the covariance matrix is first estimated from either of the received signals as:

$$\mathbf{R}^{(i)} = \mathbb{E}\left[\mathbf{x}^{(i)}[k]\mathbf{x}^{(i)^H}[k]\right] \tag{2}$$

where $(\cdot)^H$ denotes the Hermitian transpose. The related null space is then calculated as:

$$D^{(i)}(\theta) = \mathbf{a}^{(i)^H}(\theta)\{\mathbf{E}_N^{(i)}\mathbf{E}_N^{(i)^H}\}\mathbf{a}^{(i)}(\theta) \tag{3}$$

where $\mathbf{E}_N^{(i)}$ is the matrix that contains the noise eigenvectors of $\mathbf{R}^{(i)}$. The MUSIC pseudo spectrum is then determined as:

$$P^{(i)}(\theta) = \frac{1}{D^{(i)}(\theta)} \tag{4}$$

Examples of obtained pseudo spectra with $D = 2$ correlated sources are shown in Fig. 3 (simulation conditions given in the caption). When using 1 000 snapshots (Fig. 3a), the two largest peaks in the pseudo spectrum calculated from either of the ports corresponds to the two DoA ($\theta_1 = -58°$ and $\theta_2 = 26°$). However, spurious peaks, due to the multiple beams existing at each frequency, are also visible. When the number of snapshots decreases to 50 as in Fig. 3b, the largest peaks are not necessarily corresponding to the true DoA. Even worst, the port 1 pseudo spectrum does not exhibit any peak at $\theta_1 = -58°$, which jeopardizes the robustness of the scheme.

IV. DoA Ambiguities Mitigation

Three different techniques are considered to leverage the signals received by both signals in an attempt to improve estimation performance.

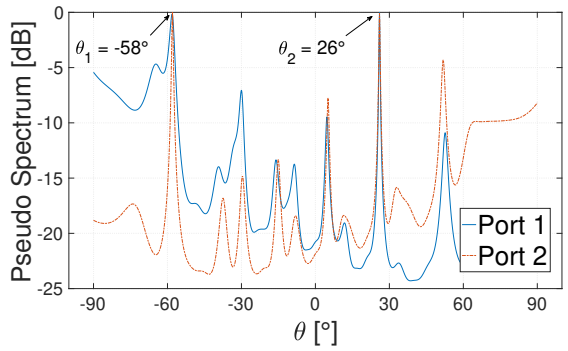

(a) 1 000 snapshots

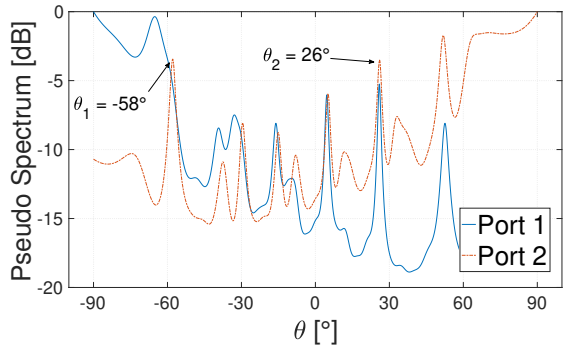

(b) 50 snapshots

Fig. 3: MUSIC pseudo spectra obtained from the received signals at port 1 and 2 of the LWA. $D = 2$ correlated ($\rho = 0.9$) sources are considered with DoA: $\theta_1 = -58°$, $\theta_2 = 26°$. SNR = 10 dB, $M = 201$ frequency samples.

A. Technique 1 (T1)

Technique 1 (T1) consists in averaging the null space calculated from each port as:

$$D^{(\mathrm{T1})}(\theta) = \frac{D^{(1)}(\theta) + D^{(2)}(\theta)}{2} \tag{5}$$

The pseudo spectrum is then calculated as:

$$P^{(\mathrm{T1})}(\theta) = \frac{1}{D^{(\mathrm{T1})}(\theta)} \tag{6}$$

B. Technique 2 (T2)

Technique 2 (T2) consists in extending the LWA manifold by concatenating the LWA response vector obtained by both ports such as:

$$\mathbf{a}^{(T2)}(\theta_d) = \begin{bmatrix} \mathbf{a}^{(1)}(\theta_d) \\ \mathbf{a}^{(2)}(\theta_d) \end{bmatrix} = \begin{bmatrix} a_1^{(1)}(\theta_d) \\ \vdots \\ a_M^{(1)}(\theta_d) \\ a_1^{(2)}(\theta_d) \\ \vdots \\ a_M^{(2)}(\theta_d) \end{bmatrix} \tag{7}$$

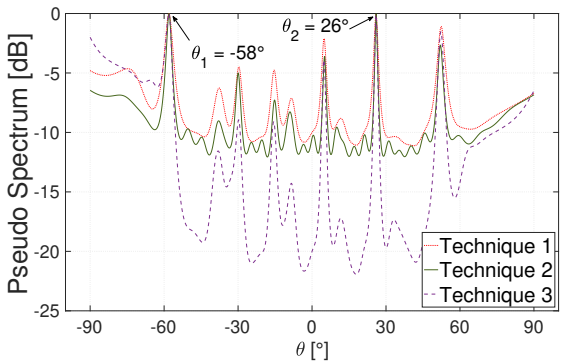

Fig. 4: MUSIC pseudo spectrum obtained with 50 snapshots using different techniques. $D = 2$ correlated ($\rho = 0.9$) sources are considered with DoA: $\theta_1 = -58°$, $\theta_2 = 26°$. SNR = 10 dB, $M = 201$ frequency samples.

Consequently, a signal vector of length $2M$ is first created thanks to received signals at both ports such as:

$$\mathbf{x}^{(T2)}[k] = \begin{bmatrix} \mathbf{x}^{(1)}[k] \\ \mathbf{x}^{(2)}[k] \end{bmatrix} \tag{8}$$

Using this signal $\mathbf{x}^{(T2)}$, a unique covariance matrix is estimated $\mathbf{R}^{T2}$ (according to eq. 2) and the corresponding pseudo spectrum $P^{T2}(\theta)$ is calculated using eq. 3, 4, and 8.

C. Technique 3 (T3)

The technique 3 (T3) uses a simple dot product between pseudo spectra calculated from received signals at both ports:

$$P^{(\mathrm{T3})}(\theta) = P^{(1)}(\theta).P^{(2)}(\theta) \tag{9}$$

D. Enhanced pseudo spectrum

An example of pseudo spectrum obtained with the three techniques is shown in Fig. 4 under the same simulation conditions as in Fig. 3b. Unlike in Fig. 3b where only one received signal was used to calculate the pseudo spectrum, all three techniques here exhibit their two largest peaks for the true DoA. This suggests that these approaches are beneficial to improve DoA estimation robustness. However, spurious peaks of non-negligible level are still observed. To assess the DoA estimation performance, Monte Carlo simulations are conducted in the next section.

V. Estimation Performance Evaluation

The complex LWA response vector $\mathbf{a}^{(i)}(\theta)$ is obtained by Ansys HFSS simulations of the structure detailed in section II using the discrete frequency solver with a frequency step of 10 MHz and an angular step of $0.1°$ to calculate the radiated far field. The same steps are used to simulate the system model described in section III, which leads to $M = 201$ frequency samples in the 26-28 GHz range and a θ grid of of $0.1°$ step for the search space. The number of snapshots varies from $K = 10$ to 1000. A signal-to-noise ratio (SNR) of 10 dB is considered. $D = 2$ correlated sources are considered with a correlation $\rho = 0.9$. The source signals follow a complex

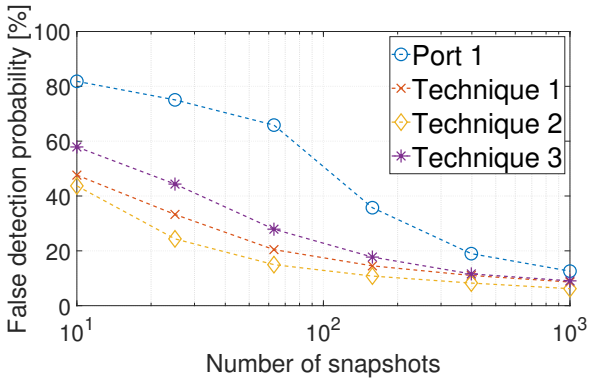

(a)

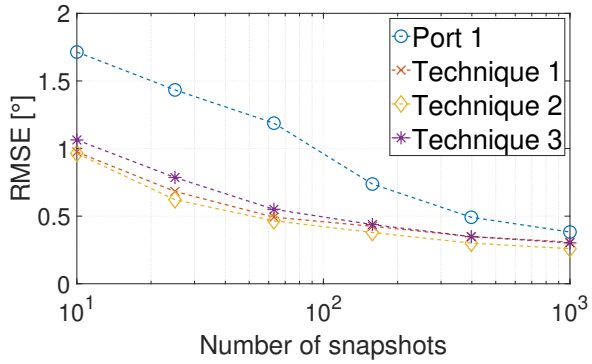

(b)

Fig. 5: Performance evaluation as a function of the number of snapshots for different ambiguity mitigation techniques with 2 correlated incoming sources ($\rho = 0.9$), SNR = 10 dB, 10 000 Monte Carlo realizations with random DoA uniformly distributed in the $-90/90°$ FoV. (a) False detection probability and (b) RMSE.

normal distribution. θ_1 and θ_2 are the DoA of the 2 sources and are modelled by random variables uniformly distributed within the $-90/90°$ FoV. 10 000 Monte Carlo realizations have been used to average the results.

The DoA estimation performance is assessed for the three techniques described in section IV and compared with the estimation performance obtained using a single port of the LWA. Fig. 5a shows the probability of false detection. A threshold of $5°$ has been arbitrary chosen to define a false detection. This value is about three times the largest root mean squared error (RMSE) calculated among all considered scenarios. As expected, the false detection probability decreases as the number of snapshots increases. It is observed that leveraging the signals received by both ports of the LWA improves the performance with all considered techniques. Technique 2 exhibits the lowest probability regardless the number of snapshots while Technique 1 outperforms Technique 3, except when the number of snapshots gets large, where both techniques performs equally.

The RMSE on the DOA is then evaluated. False detected DoA are discarded in the RMSE calculation process. Results are shown in Fig. 5b. All three techniques decrease the RMSE as compared to using only one LWA port. Technique 2 slightly outperforms the other approaches.

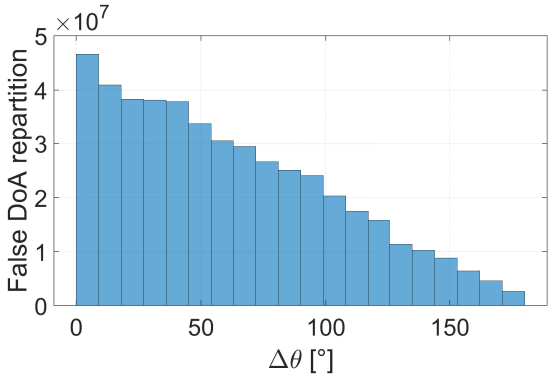

Fig. 6: Repartition of false DoA as a function of $\Delta\theta$ defined as the angular difference between the 2 sources: $|\theta_1 - \theta_2|$.

Fig. 6 shows the repartition of false DoA as a function of $\Delta\theta$, defined as the angular difference between the 2 sources DoA, i.e., $|\theta_1 - \theta_2|$. Results from all simulations in Fig. 5 using Technique 2 have been used to plot this repartition. It is observed that the false detection is more likely to occur when the two sources are close to each other. On the other hand, it was observed (not shown here) that false detection does not depend on the actual DoA values. This is thanks to the good FoV coverage achieved by both LWA ports, i.e., the SNR does not drop significantly towards end-fire when exploiting both antenna ports.

VI. Conclusion

This paper proposes and assesses three techniques to efficiently making use of received signals from both ports of 1-D frequency beam scanning leaky-wave antennas (LWA) using MUSIC algorithm. The goal is to reduce direction of arrival (DoA) ambiguities that arise with multibeam LWA, which operate using multiple fast spatial harmonics to reduce the frequency bandwidth required to estimate DoA over the whole $180°$ field of view. It was found that increasing the LWA manifold by concatenating both port responses performs the best. In particular, using a 2 GHz bandwidth about 27 GHz, a false detection probability lower than 15% was obtained for 2 correlated ($\rho = 0.9$) incoming sources using 100 snapshots and with an SNR of 10 dB.

Acknowledgment

This work was supported by the ANR BeSensiCom project, grant ANR-22-CE25-0002 of the French Agence Nationale de la Recherche, and carried out in the framework of COST Action CA20120 INTERACT.

References

[1] F. Demmel, "Practical Aspects of Design and Application of Direction-Finding Systems," in *Classical and Modern Direction-of-Arrival Estimation*, T.E. Tuncer and B. Friedlander, Ed. Academic Press, Boston, 2009, ch. 2, doi: https://doi.org/10.1016/B978-0-12-374524-8.00008-8.

[2] B. Friedlander, "Wireless Direction-Finding Fundamentals," in *Classical and Modern Direction-of-Arrival Estimation*, T.E. Tuncer and B. Friedlander, Ed. Academic Press, Boston, 2009, ch. 1, doi: https://doi.org/10.1016/B978-0-12-374524-8.00001-5.

[3] A. A. Oliner and D. R. Jackson, "Leaky-wave antennas," in *Antenna Engineering Handbook*, J. Volakis, Ed. New York: McGraw-Hill, 2007, ch. 11.

[4] Q. Zhang, J. Sarrazin, M. Casaletti, G. Valerio, P. De Doncker, A. Benlarbi-Delai, "Enhanced Scanning Range Design for Leaky-Wave Antenna (LWA) at 60 GHz", 13th European Conference on Antennas and Propagation (EuCAP), Krakow, Poland, 1-5 April 2019

[5] X. Zeng, Q. Chen, O. Zetterstrom, and O. Quevedo-Teruel, "Fully Metallic Glide-Symmetric Leaky-Wave Antenna at Ka-Band With Lens-Augmented Scanning," in IEEE Transactions on Antennas and Propagation, vol. 70, no. 8, pp. 7158-7163, Aug. 2022, doi: 10.1109/TAP.2022.3146855.

[6] A. Gil-Martinez, J. A. López-Pastor, M. Poveda-García, A. Algaba-Brazález, D. Cañete-Rebenaque and J. L. Gómez-Tornero, "Monopulse Leaky-Wave Antennas for RSSI-based Direction Finding in Wireless Local Area Networks," in IEEE Transactions on Antennas and Propagation, doi: 10.1109/TAP.2023.3313161.

[7] J. L. Gómez-Tornero, A. Gil Martínez, M. Poveda-García and D. Cañete-Rebenaque, "ARIEL: Passive Beam-Scanning Antenna teRminal for Iridescent and Efficient LEO Satellite Connectivity," in IEEE Antennas and Wireless Propagation Letters, vol. 21, no. 11, pp. 2268-2272, Nov. 2022, doi: 10.1109/LAWP.2022.3193040.

[8] J. Sarrazin, "MUSIC-based Angle-of-Arrival Estimation using Multibeam Leaky-Wave Antennas," URSI GASS 2021, Rome, Italy, 28 August - 4 September 2021

[9] J. Sarrazin and G. Valerio, "Multibeam Leaky-Wave Antenna for Mm-wave Wide-Angular-Range AoA Estimation," 2022 16th European Conference on Antennas and Propagation (EuCAP), 2022, pp. 1-5, doi: 10.23919/EuCAP53622.2022.9769571.

[10] J. Sarrazin and G. Valerio, "H-Plane-Scanning Multibeam Leaky-Wave Antenna for Wide-Angular-Range AoA Estimation at mm-wave," 2023 17th European Conference on Antennas and Propagation (EuCAP), Florence, Italy, 2023, pp. 1-4, doi: 10.23919/EuCAP57121.2023.10133492.